Diode-Based HVdc Link for the Connection of Large Offshore Wind Farms

Ramon Blasco-Gimenez, *Senior Member, IEEE*, Salvador Añó-Villalba, Johel Rodríguez-D'Derlée, *Student Member, IEEE*, Soledad Bernal-Perez, and Francisco Morant

***Abstract*—This paper includes a technical feasibility study on the use of diode-based HVdc links for the connection of large offshore wind farms based on synchronous generators. A technique for the voltage and frequency control of the offshore ac grid is presented. The proposed control technique allows the operation of the rectifier end of the HVdc link in current or voltage control mode. Fault response to onshore voltage sags of up to 80% has been shown to be comparable to that of thyristor-based rectifiers. Moreover, the complete system shows an adequate fault-ride-through operation to solid short circuits at onshore inverter terminals. PSCAD® simulations are used to prove the technical feasibility of the proposed control techniques both in steady state and during transients.**

***Index Terms*—Current control, frequency control, HVdc transmission control, power generation control, voltage control, wind power generation.**

I. Introduction

THE USE of single generators connected to diode-based HVdc rectifiers has been proposed in the past for unidirectional power links [1]–[5] . The use of an uncontrolled rectifier for the HVdc link presents several advantages over standard thyristor-based HVdc links, namely, lower conduction losses, lower installation costs, and higher reliability, as gate drivers are no longer needed for the rectifier converter. Moreover, if the generators are directly connected to the diode rectifiers, the use of a rectifier transformer might be avoided [2].

In spite of the aforementioned advantages, diode rectifier-based HVdc links exhibit important drawbacks. For instance, these kinds of rectifiers can only be operated in voltage control mode, the voltage being regulated by generator excitation [2]. Therefore, HVdc-link current control must be provided by the inverter, increasing the probability of inverter commutation failure and decreasing overall efficiency. Behavior during transients and recovery time is also of concern. Even if the transient inductance of the generator can be increased in order to limit rectifier overcurrent during faults, relatively long recovery times (around 1.5 s) have been reported [1]. These drawbacks, together with the fact that most HVdc links require bidirectional power flow, have been important deterrents to the use of diode rectifier for HVdc links.

On the other hand, HVdc lines are being used or projected for the connection of large offshore wind farms located at distances greater than 50 or 60 km from the coastline. At such distances, an ac connection is no longer viable, and hence, the power connection to the onshore transmission grid has to be carried out using HVdc lines. Current techniques include the use of voltage source converters (VSC) for powers around or below 500 MW [6]–[10] , whereas the transmission of higher power at higher voltage levels still requires the use of line-commutated converters (LCC) [11].

Alternatively, the use of offshore dc grids has been proposed [12]; however, the dc voltages attainable at the wind turbine terminals are still comparatively small for effective HVdc transmission.

The connection of large wind farms using diode-based HVdc links is of particular interest, as the power flow is unidirectional and the wind turbine power electronic converters can be used to mitigate the previously mentioned diode rectifier drawbacks.

In any case, LCC-HVdc-connected wind farms require an adequate control of the offshore ac-grid voltage and frequency to ensure proper operation of the offshore line-commutated rectifier (both for controlled or uncontrolled rectifiers). Several alternatives have been proposed for the voltage and frequency control of offshore ac grids using wind turbines based on doubly fed induction generators [13], [14], directly connected induction generators [15], or optimization techniques [16] together with LCC-HVdc links. Some techniques make use of an offshore STATCOM for this purpose [17]. The aforementioned techniques rely on the rectifier firing angle to control directly or indirectly the offshore grid voltage and frequency. Therefore, these techniques are no longer valid when an uncontrolled rectifier is used.

On the other hand, an increased number of wind turbine manufacturers are opting for the use of synchronous generator (SG)-based wind turbines with fully rated converters, either direct-drive or with a single-stage gearbox. The reduction in power electronic costs, more stringent grid regulations, and reliability problems of three-stage gearboxes being the main reasons for

Manuscript received May 25, 2010; revised September 24, 2010 and December 17, 2010; accepted January 31, 2011. This work was supported in part by the Spanish Ministry of Science and Technology and in part by the European Union FEDER funds under Grants DPI2007-64730 and DPI2010-16714. Paper no. TEC-00234-2010.

R. Blasco-Gimenez and F. Morant are with the Department of Systems Engineering and Control, Universidad Politécnica de Valencia, Valencia 46022, Spain (e-mail: r.blasco@ieee.org; fmorant@isa.upv.es).

S. Añó-Villalba and S. Bernal-Perez are with the Department of Electrical Engineering, Universidad Politecnica de Valencia, Valencia 46022, Spain (e-mail: sanyo@die.upv.es; sbernal@die.upv.es).

J. Rodríguez-D'Derlée is with the Institute of Control Systems and Industrial Computing, Universidad Politecnica de Valencia, Valencia 46022, Spain (e-mail: jdderlee@ieee.org).

Color versions of one or more of the figures in this paper are available online at http://ieeexplore.ieee.org.

Digital Object Identifier 10.1109/TEC.2011.2114886

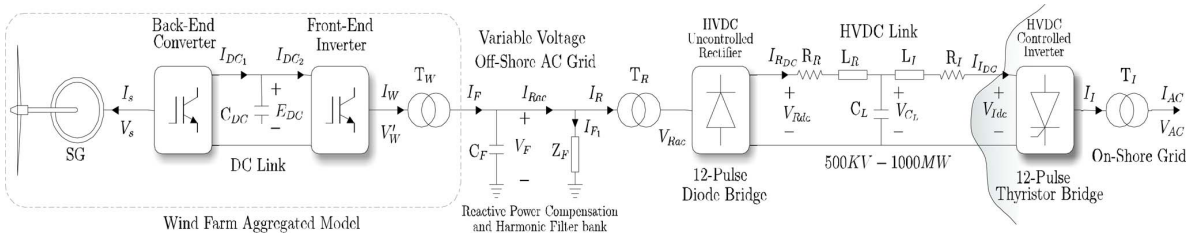

Fig. 1. SG-Based offshore wind farm with HVdc connection.

this change in technology. Currently, installed SG-based wind turbines are rated up to 6 MW [18], [19].

This paper presents a technical feasibility study on the use of diode-based HVdc rectifiers for the connection of large offshore SG-based wind power plants. A novel control algorithm is presented for the regulation of the offshore ac-grid voltage, frequency, and delivered power, while keeping optimal energy extraction on each wind turbine.

The proposed control approach allows the combination of wind farm and diode rectifier to operate either in voltage control mode or in current control mode, in line with standard practice in fully controlled LCC-HVdc links.

Moreover, the overall system shows good behavior during offshore faults, being able to control after fault HVdc-link currents in around 100 ms from the onset of the short circuit.

II. System Modeling and Control

Fig. 1 shows a diagram of the complete system under consideration. Energy is extracted by the SG-based wind turbines, rectified by the back-end converter, and then injected into the offshore ac grid through the front-end inverter. The voltage is stepped up by the wind turbine transformer T_W for the connection to the offshore ac grid. The HVdc rectifier station is modeled considering a 12-pulse uncontrolled rectifier, with the corresponding transformer T_R and filter bank (C_F, Z_F) for reactive power compensation and harmonic filtering.

The wind farm considered is a 1-GW aggregated model of a direct drive permanent magnet 80 pole-pair SG machine with mechanical and electrical parameters extrapolated from [20]. The SG is controlled using field-oriented control [21], [22], with the field current reference set to zero $(I^*_{sd} = 0)$ for maximum torque per amp operation.

As the offshore HVdc uncontrolled rectifier does not actively contribute to regulate the offshore ac-grid voltage, the control of the wind turbines is carried out assuming a stand-alone generator system. Therefore, the wind turbine front-end inverter active current cannot be used for the control of the wind turbine dc-link, as is common practice [18], [23].

Alternatively, the control method shown in Fig. 2 will be used, where the back-end converter I_{sq} current is used for the control of the dc-link voltage $E_{\rm dc}$ [24]. The specific details and the performance of such control strategy can be found in [25].

The HVdc link is modeled using a Γ-equivalent of the dc transmission line. The onshore inverter station is modeled by a variable voltage dc source, since the onshore inverter would

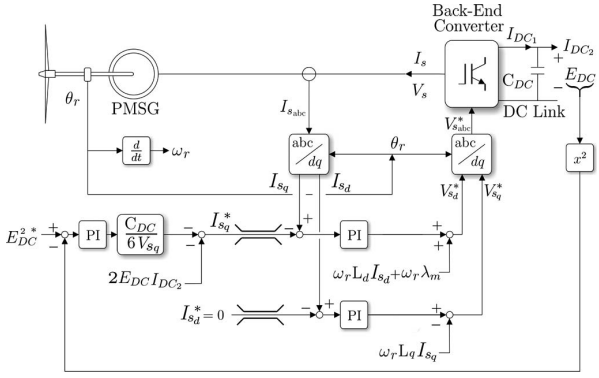

Fig. 2. Wind turbine control system.

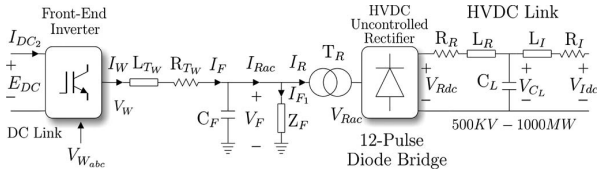

Fig. 3. Offshore wind farm simplified model.

determine the voltage $V_{\rm Idc}$ when controlled on a minimum$-\gamma$ or constant voltage strategy [13], [26].

Fig. 3 shows the simplified model of the offshore wind farm depicted in Fig. 1. Note that the voltage drop caused by the onshore inverter transformer leakage inductance in T_I is not considered.

The analysis of the offshore ac grid shown in Fig. 1 has been carried out under the following simplifying assumptions.

1) Offshore ac line impedance is negligible with respect to wind turbine transformer leakage impedance.
2) Transformer shunt branches are not considered.

Considering these assumptions, the ac-grid dynamics of the simplified model in Fig. 3, expressed in a synchronous frame oriented on V_F, i.e., $V_{Fq} = 0$, are

$$\frac{d}{dt}I_{Fd} = -\frac{R_{T_W}}{L_{T_W}}I_{Fd} + \omega_F I_{Fq} + \frac{1}{L_{T_W}}V_{Wd} - \frac{1}{L_{T_W}}V_{Fd} \quad (1)$$

$$\frac{d}{dt}I_{Fq} = -\omega_F I_{Fd} - \frac{R_{T_W}}{L_{T_W}}I_{Fq} + \frac{1}{L_{T_W}}V_{Wq} \quad (2)$$

$$\frac{d}{dt}V_{Fd} = \frac{1}{C_F}I_{Fd} - \frac{1}{C_F}I_{Racd} \quad (3)$$

$$\omega_F V_{Fd} = \frac{1}{C_F}I_{Fq} - \frac{1}{C_F}I_{Racq} \quad (4)$$

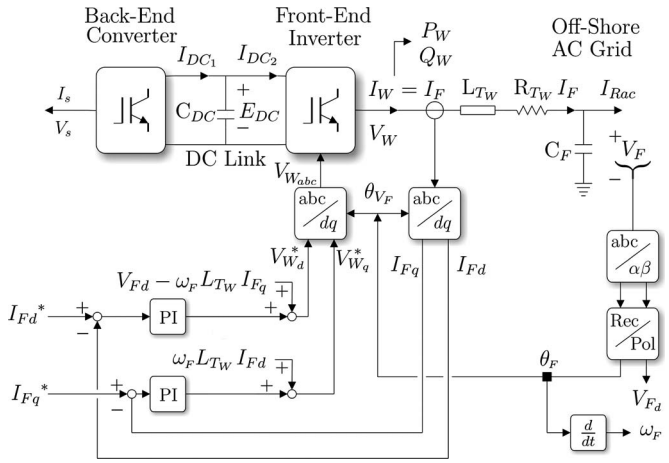

Fig. 4. Offshore I_{Fd} and I_{Fq} current control loops.

where all the variables are referred to the secondary side of T_W and ω_F is the instantaneous frequency of voltage V_F. Defining a set of decoupling inputs as

$$u_{Fd} = L_{T_W}\,\omega_F\, I_{Fq} + V_{Wd} - V_{Fd} \tag{5}$$

$$u_{Fq} = -L_{T_W}\,\omega_F\, I_{Fd} + V_{Wq} \tag{6}$$

the dynamics of (1) and (2) would be

$$\frac{d}{dt} I_{Fd} = -\frac{R_{T_W}}{L_{T_W}} I_{Fd} + \frac{1}{L_{T_W}} u_{Fd} \tag{7}$$

$$\frac{d}{dt} I_{Fq} = -\frac{R_{T_W}}{L_{T_W}} I_{Fq} + \frac{1}{L_{T_W}} u_{Fq}. \tag{8}$$

Note that all the magnitudes required for the calculation of the decoupling inputs in (5) and (6), i.e., V_{Fd}, I_{Fd}, I_{Fq}, and ω_F, can be measured locally at the terminals of the wind turbines. Hence, the front-end converter voltages can be calculated as follows:

$$V_{Wd} = u_{Fd} + V_{Fd} - L_{T_W}\,\omega_F\, I_{Fq} \tag{9}$$

$$V_{Wq} = u_{Fq} + L_{T_W}\,\omega_F\, I_{Fd}. \tag{10}$$

Therefore, it is possible to control I_{Fd} and I_{Fq} to follow desired step references I^*_{Fd} and I^*_{Fq} with simple PI controllers, as far as the wind turbine front-end converter has enough dc-link voltage ($E_{\rm dc}$) headroom and V_{Wd}, V_{Wq} do not saturate. The I_{Fd} and I_{Fq} control loops are depicted in Fig. 4.

Assuming sufficiently fast current control loops, the front-end converter currents will follow their references, i.e., $I_{Fd} = I^*_{Fd}$ and $I_{Fq} = I^*_{Fq}$. Therefore, the system dynamics are reduced to

$$\frac{d}{dt} V_{Fd} = \frac{1}{C_F} I^*_{Fd} - \frac{1}{C_F} I_{Racd} \tag{11}$$

$$\omega_F V_{Fd} = \frac{1}{C_F} I^*_{Fq} - \frac{1}{C_F} I_{Racq.} \tag{12}$$

It is important to remark that these expressions are only valid if the current loops are significantly faster than the voltage dynamics in (11) and (12).

Therefore, I^*_{Fd} can be used to control the offshore ac-grid voltage V_{Fd}, whereas I^*_{Fq} can be used as a control action for the offshore grid frequency ω_F. Note that this is the opposite to that commonly seen in power systems, where the active power is used to control the frequency and the reactive power to control the voltage.

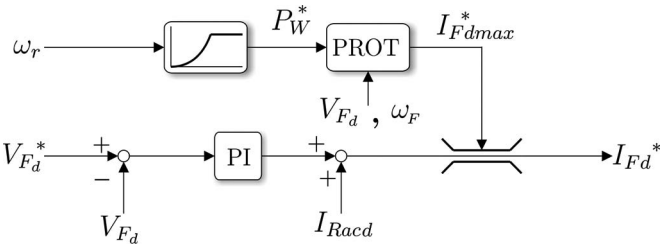

Fig. 5. Offshore ac-grid voltage control.

However, in our case, the power electronics effectively decouple the front-end converter dynamics from the primary mover. Moreover, the offshore ac grid can be considered as a stand-alone grid. Hence, the offshore grid dynamics (dominated by the capacitor bank) determine the coupling between P_W, Q_W, V_{Fd}, and ω_F. In the most general case, ac-grid characteristics are difficult to obtain; however, in the case of an offshore wind farm, the offshore ac-grid characteristics are largely determined by the transformer leakage reactance and the capacitance of the combined filter and capacitor banks. These parameters are known with reasonable accuracy.

A. *Offshore AC-Grid Voltage Control*

Fig. 5 shows the offshore ac voltage V_{Fd} control loop. When I^*_{Fd} is not saturated, the voltage PI controller will ensure that the offshore ac voltage follows its reference. If the HVdc diode rectifier is conducting, the relationship between ac and dc voltages on both sides of the rectifier is [27]

$$V_{R\rm dc} = \frac{6\sqrt{6}}{\pi} N V_{Fd} - \frac{6}{\pi} \omega_F L_{T_R} I_{R\rm dc} \tag{13}$$

where N is the rectifier transformer turns ratio, V_{Fd} represents line to neutral rms values, and L_{T_R} is the rectifier transformer leakage inductance.

Therefore, if the onshore inverter is operating in current control mode, the voltage control loop in Fig. 5 will ensure that V_{Fd} follows its reference, and hence, the rectifier side HVdc voltage will be determined by (13). This mode of operation is similar to that already reported in [2], and therefore shares the disadvantages mentioned in Section I. Clearly, when the wind farm is operating in voltage control mode, it is not possible to limit the wind turbine speed by acting on the wind farm power set point. Therefore, standard pitch control is used in order to prevent the wind turbines from overspeeding when the wind farm is operated in voltage control mode or when the wind speed is relatively high.

On the other hand, if the onshore inverter is operating in minimum$-\gamma$ or in voltage control mode, the HVdc rectifier and inverter dc voltages will be approximately the same, neglecting HVdc line voltage drop. Hence, the diode rectifier will act as a voltage clamp on V_{Fd} (13). At this point, the voltage loop in

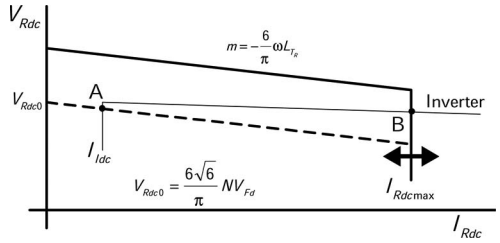

Fig. 6. Steady-state operation characteristics.

Fig. 5 will saturate and the wind farm together with the diode rectifier will be operating in current control mode.

Fig. 6 shows the steady-state operation characteristics of the HVdc link. Point A represents the case where the rectifier is operating in voltage control mode, i.e., the control loop in Fig. 5 is not saturated and the HVdc-link current is determined by the onshore inverter current control loop. If the voltage V_{Fd} is raised, then the system would operate at point B, where the wind farm active power limit has been reached, the voltage control loop is saturated, and V_{Fd} would no longer follow its reference. At this stage, the HVdc-link voltage $V_{I\mathrm{dc}}$ would be determined by the onshore inverter operating on minimum$-\gamma$ or voltage control and, in steady state, $V_{R\mathrm{dc}} = V_{I\mathrm{dc}} + (R_R + R_I)I_{R\mathrm{dc}}$. Therefore, V_{Fd} would be

$$V_{Fd} = \frac{\sqrt{6}}{36}\frac{\pi}{N}\left(V_{R\mathrm{dc}} + \frac{6}{\pi}L_{T_R}\omega_F I_{R\mathrm{dc}}\right) = \tag{14}$$

$$= \frac{\sqrt{6}}{36}\frac{\pi}{N}\left(V_{I\mathrm{dc}} + \left(R_R + R_I + \frac{6}{\pi}L_{T_R}\omega_F\right)I_{R\mathrm{dc}}\right). \tag{15}$$

Clearly, when operating at point B, the offshore ac-grid voltage V_{Fd} is determined by the onshore dc voltage $V_{I\mathrm{dc}}$ and the HVdc rectifier current $I_{R\mathrm{dc}}$. Therefore, the power delivered by the wind farm and transmitted by the HVdc link is controlled by limiting the HVdc rectifier current $I_{R\mathrm{dcmax}}$. This limit is set indirectly by the wind turbine maximum active power current $I^*_{Fd\mathrm{max}}$.

Therefore, wind turbine optimal power tracking can be achieved by considering the optimal power characteristic of the wind turbine [23]

$$P^*_{W\,(\mathrm{opt})} = K_{\mathrm{opt}}\omega_r^3 \tag{16}$$

where ω_r is the wind turbine speed and K_{opt} is an optimal constant that depends on the physical characteristics of the wind turbine rotor and the air density. At any instant of time, the active power delivered by the wind farm would be

$$P_W = \frac{1}{k_2}\left(V_{W\,d}I_{F\,d} + V_{W\,q}I_{F\,q}\right) \approx \frac{1}{k_2}V_{F\,d}I_{F\,d} \tag{17}$$

where k_2 is a constant that depends on the scaling factors used for the transformation of the electrical quantities into synchronous coordinates. In our case, voltage and current quantities are scaled to represent rms phase values; therefore, $k_2 = 1/3$. The I^*_{Fd} limit for maximum power tracking of the wind farm is, therefore, obtained by combining the two previous expressions

$$I^*_{Fd\ \mathrm{max}} = k_2\frac{P^*_{W\,(\mathrm{opt})}}{V_{Fd}} = k_2\frac{K_{\mathrm{opt}}\omega_r^3}{V_{Fd}}. \tag{18}$$

Note that this value is calculated for an aggregated model. If the different wind turbines were to be considered, then the I^*_{Fd} limit for each individual wind turbine would depend on its specific rotational speed

$$I^*_{Fdi\ \mathrm{max}} = k_2\frac{K_{\mathrm{opt}i}\omega_{ri}^3}{V_{Fd}}. \tag{19}$$

Hence, the overall wind farm active current limit would be $I^*_{Fd\ \mathrm{max}} = \sum_i I^*_{Fdi\ \mathrm{max}}$. Therefore, when the HVdc rectifier is operating in current control mode (point B in Fig. 6), the proposed control system ensures that each individual wind turbine would follow its optimal power characteristic.

Optimal power tracking is generally not possible when the wind farm and HVdc diode rectifier are operating in voltage control mode (point A in Fig. 6) as, in this case, I_{Fd} is used for the voltage control of the offshore ac grid and cannot be set to follow its optimal value (18).

It is worth stressing that the control arrangement in Fig. 5 will automatically switch between HVdc rectifier current control and voltage control depending on the mode of operation of the onshore inverter (see Fig. 6). This behavior is accomplished simply by setting adequate values for $I^*_{Fd\ \mathrm{max}}$ and V^*_{Fd}, and is consistent with standard LCC-HVdc control practice. Moreover, if the HVdc rectifier stops conducting (e.g., because of rectifier ac or dc breaker tripping), the voltage control loop will still be operational and will keep the offshore ac-grid voltage and frequency, unlike other control methods [13].

Note that the feedforward term I_{Racd} implies an impractical remote measurement of a current. The voltage control loop will still show reasonably good performance without the use of the feedforward term. Alternatively, the remote measurement can be substituted by an estimated value based on local variables.

B. Offshore AC-Grid Frequency Control

Fig. 7 shows the basic frequency control algorithm, based directly on (12) with some filtering on V_{Fd}. However, the open loop control based on (12) is extremely sensitive to C_F estimation errors and does require the use of a remote measurement of I_{Racq}. A possible solution consists on estimating the value of I_{Racq} by using local measurements

$$\hat{I}_{Racq} = \frac{1}{3}\frac{P_W V_{W\,q} - Q_W V_{W\,d}}{V_{W\,d}^2 + V_{W\,q}^2} - C_F\omega_F V_{Fd}. \tag{20}$$

Substituting (20) in (12), we have

$$I^*_{F\,q} = C_F V_{F\,d}\left(\omega^*_F - \omega_F\right) + \frac{1}{3}\frac{P_W V_{W\,q} - Q_W V_{W\,d}}{V_{W\,d}^2 + V_{W\,q}^2}. \tag{21}$$

The corresponding block diagram is shown in Fig. 8. The modified frequency control loop corresponds to a simple proportional control with a feedforward compensation term. Moreover, it is clear that the frequency control system is more robust

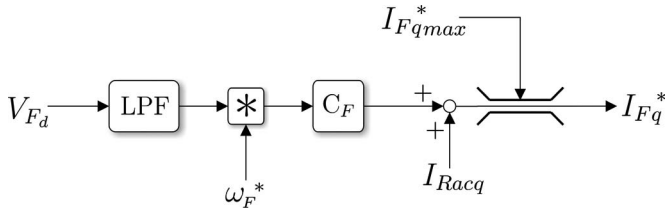

Fig. 7. Open loop offshore ac-grid frequency control.

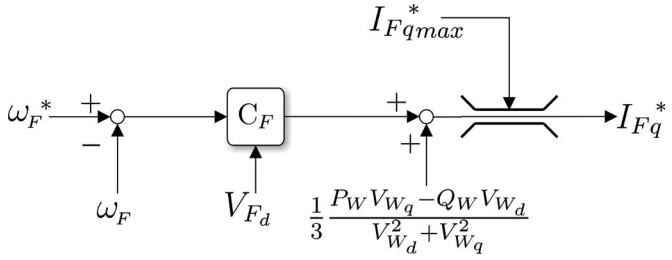

Fig. 8. Modified frequency control loop.

to C_F estimation errors, as C_F now appears within the control loop and can be considered as a loop gain, rather than a plant parameter.

Note the algebraic relationship between ω_F and the front end inverter reactive current I_{Fq} (12). Therefore, the proportional controller in Fig. 8 could, theoretically, drive ω_F to its reference instantaneously (the loop gain having only an influence on the steady-state error). In this case, the dynamics of the current loop can no longer be neglected, and hence, the closed loop ω_F dynamics are the same as those of the I_{Fd} loop. Moreover, filtering on V_{Fd} introduces additional dynamics in the frequency control loop, although such effects can be easily minimized with adequate filter design.

C. Protection and Fault-Ride-Through Operation

Wind farms of the considered size should be able to remain connected to the grid in spite of severe grid disturbances. Therefore, a protection scheme, similar to traditional voltage-dependent current order limit (VDCOL), has been included in Fig. 5.

In order to make the fault protection algorithm robust against communication failure or delays, all the variables used for protection purposes are local to the wind turbines. In this way, the maximum value of $|I_F^*|$ is determined as a function of the voltage V_{Fd}.

1) If V_{Fd} is higher than 0.5 p.u., then $|I_F^*|_{\max} = 1$ p.u.
2) If V_{Fd} is lower than 0.2 p.u., then $|I_F^*|_{\max} = 0.2$ p.u.
3) When V_{Fd} is between 0.2 and 0.5 p.u., $|I_F^*|_{\max}$ is interpolated between 0.2 and 1 p.u.

The limits for the direct and quadrature currents are obtained as follows:

$$I_{Fq\,\max}^* = |I_F^*|_{\max} \tag{22}$$

$$I_{Fd\,\max}^* = \min\left(\sqrt{|I_F^*|_{\max}^2 - I_{Fq}^2}, k_2 \frac{K_{\text{opt}}\omega_r^3}{V_{Fd}}\right). \tag{23}$$

In addition, a limit has been placed on the rate of increase of $|I_F^*|_{\max}$, in order to limit the current increase rate after the recovery of a fault.

Alternative protection schemes are possible; however, the proposed VDCOL has been chosen to show that the wind farm together with the diode rectifier can be operated in a similar way as traditional thyristor-based HVdc rectifiers.

III. Results

The validation of the previously described control strategy has been carried out using PSCAD® simulations. The parameters of the HVdc link have been obtained from the International Council on Large Electric Systems (CIGRE) benchmark model [28], using a diode rectifier instead of a thyristor rectifier and modeling the onshore inverter station by means of a variable voltage dc source to emulate an onshore inverter in voltage control mode of operation (see Fig. 3) [13], [14], [17].

The current loop bandwidth has been designed to be around 180 Hz, which is consistent with a wind turbine front-end converter operating at 1-kHz switching frequency.

A. Offshore AC-Grid and HVDC-Link Start-Up Operation

Fig. 9 shows the start-up operation of the offshore ac grid. Clearly, the HVdc diode rectifier or, in general, an LCC rectifier cannot start the offshore ac grid by itself, even if the HVdc link is energized. Therefore, the wind farm should perform this operation. Initially, the offshore inverter energizes the HVdc link and ramps up $V_{R\text{dc}}$. Once the HVdc voltage has reached its rated value, the voltage and frequency control loops of the wind farm are enabled and the voltage reference V_{Fd}^* is ramped up to 1.1 p.u. in 1.7 s. Note that the wind farm reactive current increases as the offshore ac-grid voltages reaches its rated value. This is due to the fact that the HVdc rectifier is not yet conducting, and therefore, the reactive power delivered by the capacitor bank is absorbed by the wind farm. Once V_{Fd} reaches the value $(\sqrt{6}/36)(\pi/N)V_{R\text{dc}}$ (at $t = 1.7$ s), the HVdc diode rectifier starts conducting and I_{Fd} and $I_{R\text{dc}}$ increase to their rated values. At the same time, I_{Fq} decreases as now the capacitor bank reactive power compensates the reactive power absorbed by the leakage reactance of transformer T_R and by the overlap angle of the HVdc rectifier. Note the reduction of $I_{Fd\,\max}^*$ when I_{Fq} increases to keep the allowable output current below its rated level, as per (23).

When operating at rated V_{Fd} voltage, the active power delivered by the wind farm P_W is roughly proportional to wind farm active current I_{Fd}. During operation at rated power, the wind farm delivered reactive power is zero. Fig. 9 also shows the waveforms corresponding to phase r of V_F and the ac-side currents of the diode bridge I_R.

Fig. 10 shows a detail of the previously shown start-up transient. When V_{Fd} reaches a value of 0.9 p.u. (at $t = 1.7$ s), the offshore rectifier starts conducting and currents I_{Fd} and $I_{R\text{dc}}$ increase. As current $I_{R\text{dc}}$ increases, the $V_{R\text{dc}}$ ripple increases due to the higher harmonic content at higher currents. When I_{Fd} reaches its limit ($I_{Fd\,\max}$) at $t = 1.89$ s, the voltage

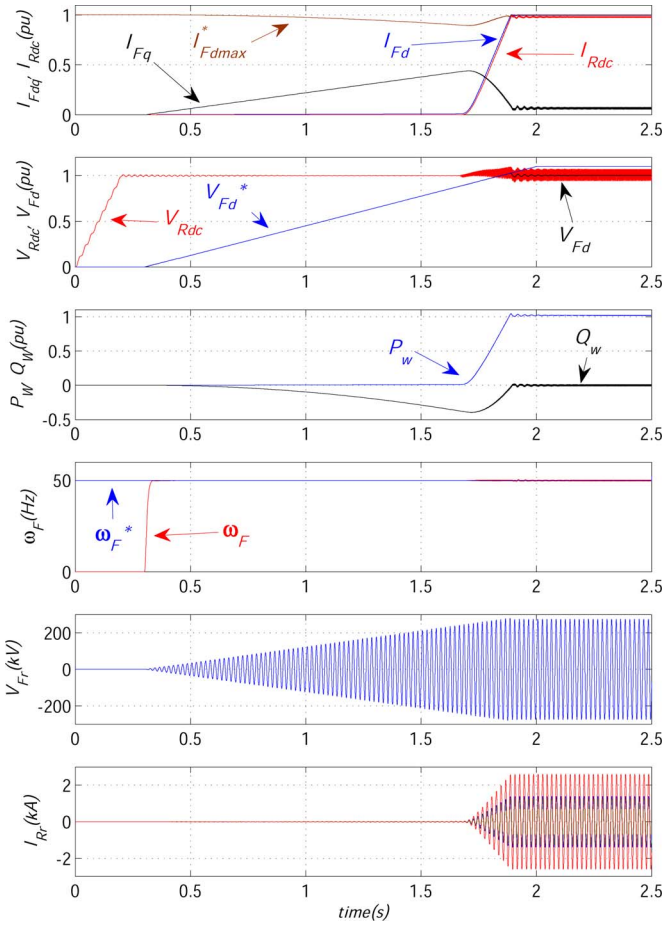

Fig. 9. Offshore grid black-start operation.

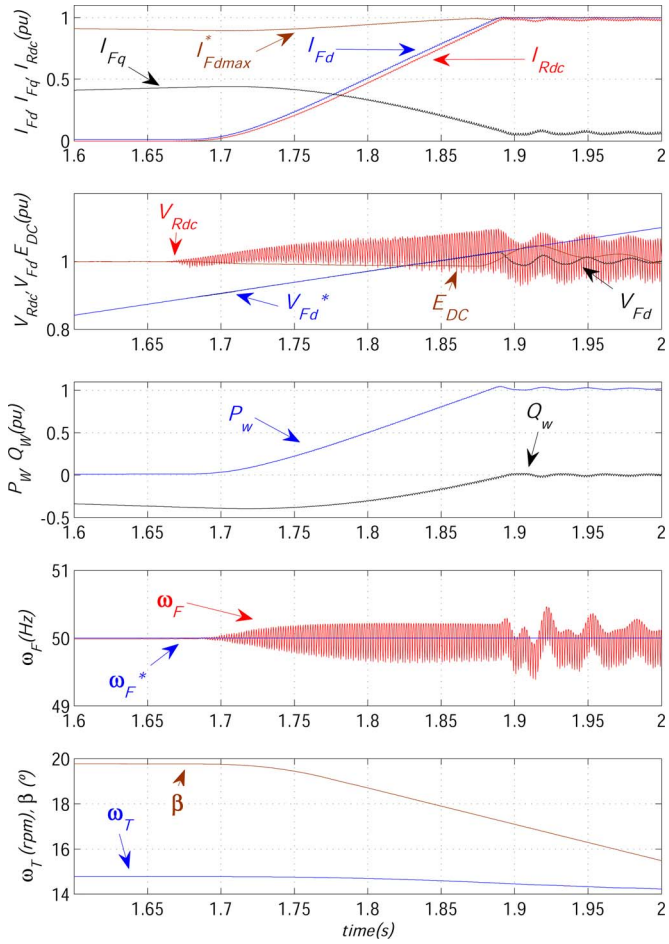

Fig. 10. Response to offshore ac voltage reference ramp.

control loop in Fig. 5 saturates and the offshore grid voltage V_{Fd} does no longer follow its reference. Therefore, Fig. 10 shows a smooth transition between voltage and current control mode of operation.

The ac-grid frequency remains close to 50 Hz during the voltage ramp-up. However, once the rectifier starts conducting, the offshore ac voltage shows an increased harmonic content, which causes the frequency and HVdc-link voltage ripple in Fig. 10. When the diode rectifier is not conducting, the wind turbine speed ω_T is kept at its rated value 14.8 rpm by means of pitch control. Once the HVdc link starts conducting, active power is extracted from the wind farm causing a small drop in wind turbine speed. At this point, the pitch angle of the wind turbine β is reduced at its maximum rate. During the connection transient, the minimum wind turbine speed is 13.5 rpm. After the minimum pitch angle is reached ($\beta = 0^o$), the wind turbine speed returns to 14.8 rpm. The wind speed during the transient is 11.48 m/s.

The transients in Figs. 9 and 10 show reliable steady-state operation at rated power. Moreover, before the HVdc diode rectifier starts conducting, the proposed control algorithm shows an excellent stand-alone operation, with good voltage and frequency regulation.

B. Response to Frequency Changes at Rated Power

The performance of the frequency control loop is shown in Fig. 11. The system is operating in current control mode at rated power. At $t = 0.1$ s, the frequency demand rises to 52 Hz (1.04 p.u.) and then is changed back to 50 Hz (at $t = 0.3$ s). A similar transient is carried out, but now reducing the frequency demand to 48 Hz. The behavior of the control system is remarkable as the actual frequency reaches its reference value in around 12 ms. The rest of the magnitudes remain constant during the transients. Only minor variations on I_{Fq}, V_{Fd}, and Q_W can be appreciated. These variations are due to the frequency-dependent nature of the reactive power of the capacitor bank, filters, and leakage reactances.

C. Wind Farm Power Control

Fig. 12 shows the response of the system to changes in the wind farm power set point. The value of $I^*_{Fd\,\max}$ in Fig. 5 has been reduced from 1 to 0.1 p.u. in 0.3 s and then ramped up to 1 p.u. to simulate power variations for changing wind conditions.

Note that I_{Fq} increases as I_{Fd} decreases, since the capacitor bank is overcompensating the reactive power absorbed by the rectifier transformer leakage reactance. This fact is consistent

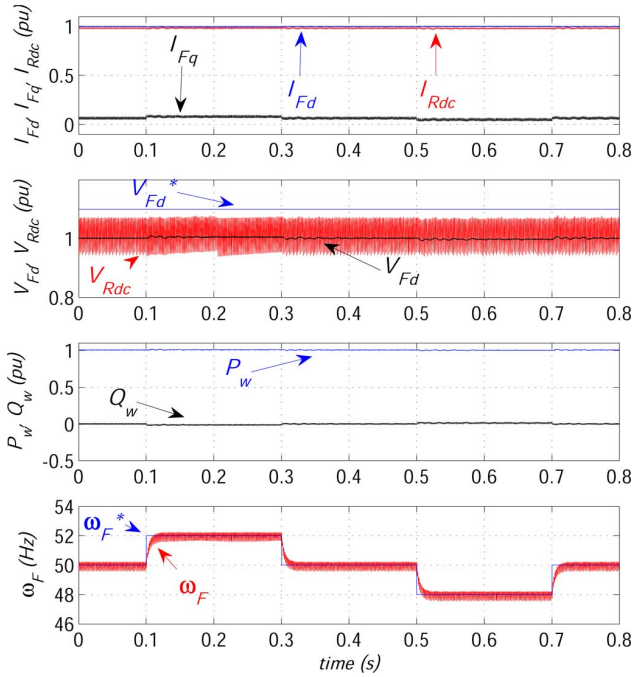

Fig. 11. Response to frequency demand changes at rated power.

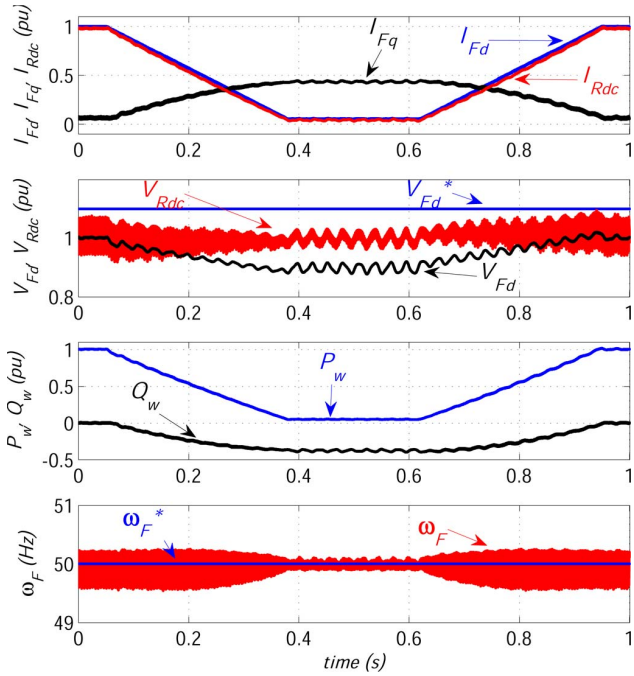

Fig. 12. Response to changes in wind farm power set point.

with the increased Q_W absorption shown in the third graph. On the other hand, the HVdc link and offshore ac-grid voltages decrease slightly along with I_{Fd} due to smaller voltage drop on the HVdc-link resistance and rectifier transformer leakage reactance. It is worth noticing the decreased harmonic content in the HVdc-link voltage V_{Rdc} at reduced power levels. During the complete transient, the offshore ac-grid frequency is kept very close to its reference value.

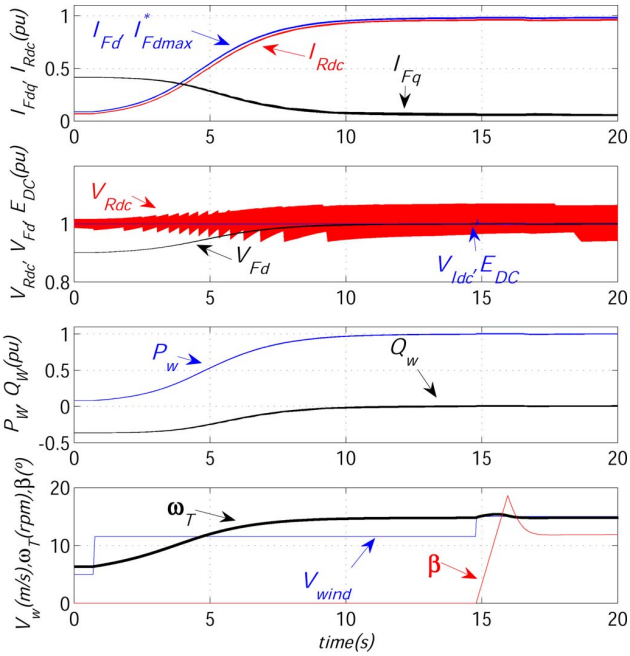

Fig. 13. Optimal power tracking.

Note that a 0.9 p.u. power transient in 0.3 s might not be realistic, as power generated from a wind farm of this size does not vary so rapidly. Nevertheless, Fig. 12 shows an excellent behavior of the proposed control system during power reference changes.

Optimal power tracking for different wind conditions is shown in Fig. 13. From an initial value of 5 m/s, the wind speed is increased to rated wind speed 11.48 m/s. The wind turbine rotational speed increases to reach rated speed and rated power operation. At $t = 14$ s, the wind speed is further increased to 15 m/s to illustrate pitch angle β control at high wind speed.

D. Fault-Ride-Through Performance During Onshore Faults

Fig. 14 shows the response of the system to a three-phase onshore grid short circuit at the inverter terminals. The fault has a duration of 400 ms, a 100% depth, and a 100-ms recovery time to 100% of the prefault voltage. During the fault, the VDCOL mechanism reduces I_{Fd} and I_{Fq} due to the small V_{Fd} values caused by the fault. As a result, the HVdc-link current (I_{Rdc}) decreases following the link unforced dynamics.

The behavior of the HVdc-link current has been analyzed theoretically assuming a short circuit at the onshore inverter terminals and an instantaneous voltage reduction at the offshore rectifier terminals. The HVdc-link natural (unforced) response can be expressed as follows:

$$I_{\mathrm{Rdc}} = 2e^{-(R/L)t} + \frac{1000\sqrt{C}}{\sqrt{8L - CR^2}} e^{-(R/2L)t} \sin \omega_n t \quad (24)$$

$$I_{\mathrm{Idc}} = 2e^{-(R/L)t} + \frac{1000\sqrt{C}}{\sqrt{8L - CR^2}} e^{-(R/2L)t} \cos \omega_n t \quad (25)$$

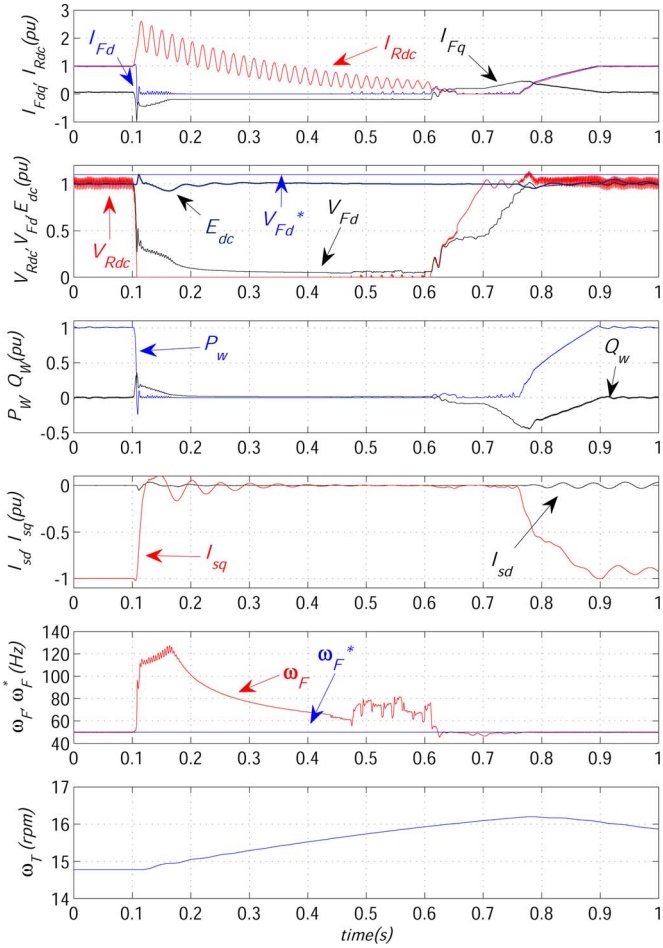

Fig. 14. Response to a three-phase fault at onshore inverter terminals.

where *R*, *L*, and *C* are the HVdc characteristic parameters and

$$\omega_n = \frac{1}{2}\sqrt{\frac{8}{LC} - \frac{R^2}{L^2}}. \tag{26}$$

Therefore, the maximum rectifier (and inverter) current will be

$$\hat{I}_{\mathrm{Rdc}} \simeq 2 + \frac{1000\sqrt{C}}{\sqrt{8L - CR^2}} \tag{27}$$

Substituting the *R*, *L*, and *C* values used in the CIGRE benchmark yields $\omega_n = 57$ Hz and $\hat{I}_{\mathrm{Rdcpeak}} = 4.33$ kA $= 2.17$ p.u. These values are consistent with the results in Fig. 14. Note that the peak current is slightly higher in Fig. 14 ($\hat{I}_{\mathrm{Rdc}} \simeq 2.5$ p.u.) as the rectifier side dc voltage does not decrease to zero instantaneously. Clearly, in order to reduce $\hat{I}_{\mathrm{Rdc}}$, a good option would be an increased value of the serial smoothing reactance. However, such an increase will lead to longer current decay times (24). On the other hand, an increase on the cable capacitance will lead to larger maximum values of I_{Rdc}. Note that the present analytical study is also valid for HVdc-link short circuits at the dc inverter terminals when VSC are used.

It is clear, both from the transient in Fig. 14 and from (24), that the amount of time the rectifier current remains above its rated value is substantially higher than that obtained with an offshore controlled rectifier.

At this stage, it is necessary to check if both $\hat{I}_{\mathrm{Rdc}}$ and $\int I^2_{\mathrm{Rdc}}dt$ are within the operational limits of existing diodes and thyristors. For calculation simplicity, it is assumed that

$$I_{\mathrm{Rdc}} = I_{\mathrm{Rdc}\infty} + \left(\hat{I}_{\mathrm{Rdc}} - I_{\mathrm{Rdc}\infty}\right) e^{-(R/2L)t}. \tag{28}$$

Therefore,

$$\int_0^T I^2_{\mathrm{Rdc}}dt = I^2_{\mathrm{Rdc}\infty}T + \frac{4LI_{\mathrm{Rdc}\infty}\left(\hat{I}_{\mathrm{Rdc}} - I_{\mathrm{Rdc}\infty}\right)}{R} + \frac{L\left(\hat{I}_{\mathrm{Rdc}} - I_{\mathrm{Rdc}\infty}\right)^2}{R} \tag{29}$$

assuming T is large enough for the current to reach a new steady-state current ($i_{\mathrm{Rdc}\infty}$). With $T = 0.4$ s, $\hat{I}_{\mathrm{Rdc}} = 5$ kA, and $I_{\mathrm{Rdc}\infty} = 0$ kA, we have $\int I^2_{\mathrm{Rdc}}dt = 5.99 \times 10^6$ A^2·s.

Both $\hat{I}_{\mathrm{Rdc}}$ and $\int I^2_{\mathrm{Rdc}}dt$ are within the operational limits of current high-power diodes and thyristors. For example, high-power thyristors of 6 kV/2.5 kA have instantaneous maximum currents of more than 35 kA and values of $\int I^2_{\mathrm{Rdc}}dt$ in excess of 9×10^6 A^2·s.

Therefore, the proposed control system allows for the power electronic devices to remain within their operational limits during solid three-phase onshore faults at inverter terminals. The system resumes operation at rated power 200 ms after the fault has been cleared. Note that the duration of the fault has been deliberately extended so the natural discharge of the HVdc link can be appreciated.

The VDCOL protection system brings the offshore ac voltage to a very low value during the fault. Therefore, the wind turbines should be able to continue their operation in the presence of low V_F voltages.

During the transient, the proposed control strategy keeps currents I_F and I_s within safe bounds. Moreover, E_{dc} overvoltage is kept below 1.1 p.u. by using dynamic braking. Additionally, wind turbine speed is limited by means of standard pitch control, reaching a maximum of 16.3 r/min. These characteristics contribute to the wind turbine required low voltage ride-through performance.

Fig. 15 shows the behavior of the system to a 0.8 p.u. voltage sag of 100-ms duration at the onshore inverter terminals. In this case, the behavior of the system is different from that shown in Fig. 14, as the control system is capable of keeping I_{Rdc} below 2 p.u. while reducing it to 0.2 p.u. in less than 50 ms.

It is worth noticing that I_{Fq} reaches its limit during the transient. Therefore, the offshore grid frequency is no longer controlled and frequencies of up to 125 Hz are observed. However, these frequencies correspond mainly to the highly distorted voltages that appear at the onset of the transient. After approximately 75 ms, the frequency control loop is no longer saturated and the frequency returns rapidly to 50 Hz.

At the onset of the transient, the power delivered by the wind farm P_W becomes negative, implying an in-flowing power to the wind turbine converters. The in-flowing power would then create

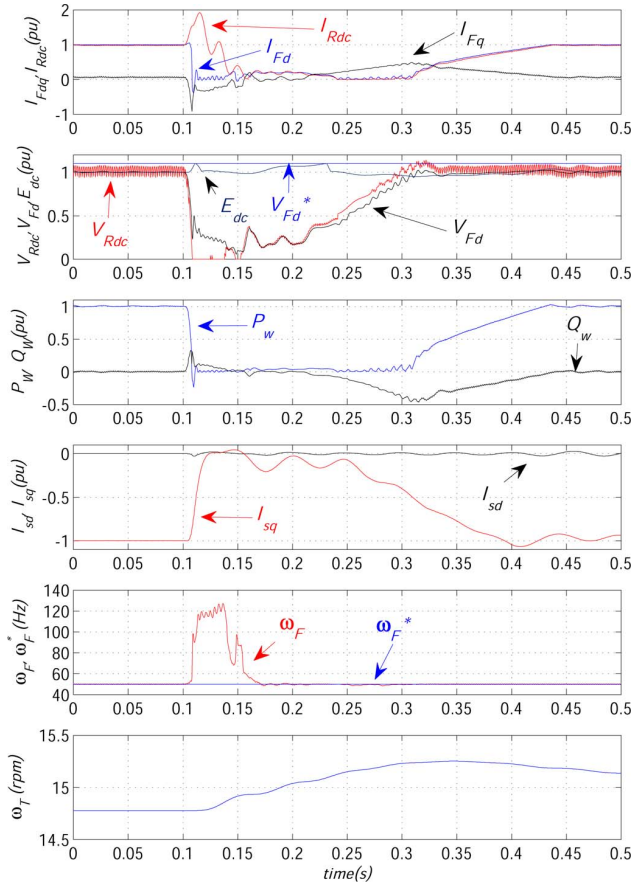

Fig. 15. Response to a 0.8 p.u. voltage sag at onshore inverter terminals.

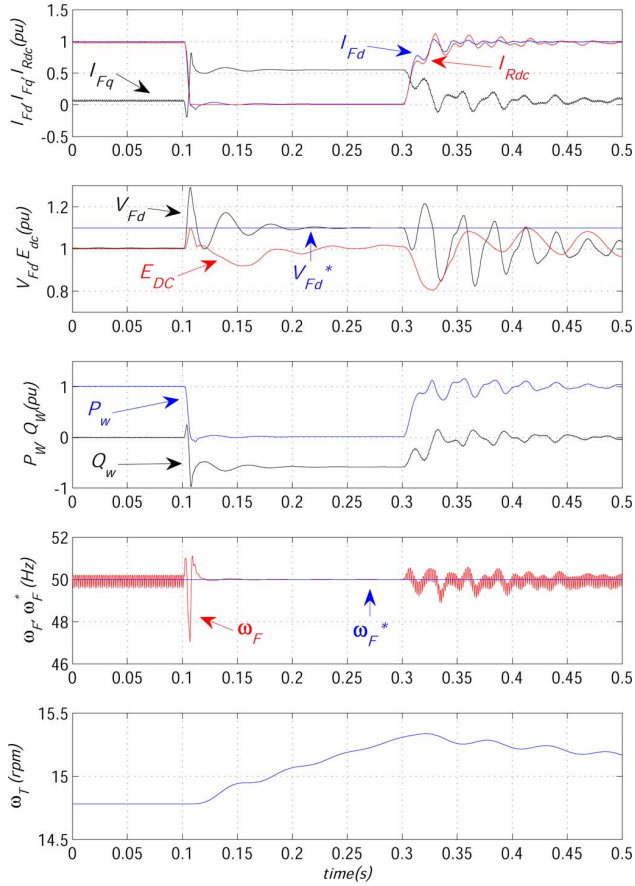

Fig. 16. Response to operation of the diode rectifier ac breaker.

a momentary increase in the wind turbine dc-link voltage $E_{\rm dc}$. As the energy absorbed by the wind turbine is small, standard protection schemes based on dynamic braking are sufficient to keep $E_{\rm dc}$ within reasonable bounds.

The overall transient, including restoration of rated power delivery lasts for around 350 ms, which is comparable to that obtained with thyristor-controlled rectifiers.

E. Voltage and Frequency Control During Rectifier AC Breaker Operation

Some of the previously reported offshore frequency and voltage control strategies use the HVdc rectifier firing angle or the HVdc current $I_{R\rm dc}$ as control actions [13]. However, these control actions are no longer available after the rectifier ac breaker has tripped. In this situation, control of the offshore grid might be lost and power transmission would not be restored at breaker reclosure.

Fig. 16 shows the behavior of the proposed control system when the rectifier ac breaker is opened at $t = 0.1$ s and reclosed after 200 ms. When the breaker trips, I_{Fd} drops to a value close to zero, and the voltage control loop shown in Fig. 5 is no longer saturated. Therefore, the offshore grid voltage is controlled to its 1.1 p.u. reference. Note that the 1.3 p.u. peak of V_{Fd} during 15 ms has to be within the design ratings of the wind turbine converters.

When the breaker is reclosed, power transmission is resumed in less than 40 ms. Note that the I_{Fd} reference has not been ramped up, as in the previous cases, giving rise to the voltage and current oscillations seen in Fig. 16 after reconnection.

During the transient, the wind turbine dc-link voltage $E_{\rm dc}$ voltage is again kept below 1.1 p.u. by means of dynamic braking. After the ac-breaker reclosure, $E_{\rm dc}$ exhibits marked oscillations at the resonant frequency of the wind turbine two-mass mechanical model. These oscillations could be mitigated by an enhanced design of the $E_{\rm dc}$ control loop or simply by using a rate limit on I_{Fd}.

IV. Discussion and Conclusion

This paper has introduced a new control system for the integrated control of an offshore wind farm, the offshore ac grid, and a diode-based HVdc link. This study aims at proving the technical feasibility of the use of a diode rectifier together with a large offshore wind farm based on fully rated converters.

The advantages of using a diode rectifier for offshore wind farms are evident, as the converter and filters are smaller, the reliability is increased as no gate drivers nor transformer tap changers are required. At the same time, the offshore converter increases its efficiency, reducing the need for cooling.

The control of the offshore ac grid is carried out in a similar way as a stand-alone system. In the proposed configuration, the

turbine back-end inverter provides control for the wind turbine dc-link voltage $E_{\rm dc}$. Therefore, the front-end inverter currents can be controlled in a voltage-oriented frame to provide a variable voltage and frequency offshore ac grid.

It is worth noticing that the proposed control system does not require the presence of an additional voltage source to set either the voltage or frequency for the voltage orientation. The proposed control system shows a voltage-closed loop bandwidth of around 20 Hz and a closed-loop frequency response of around 12 ms. These figures compare favorably to previously reported research [13].

The combination of wind farm and HVdc diode rectifier can be operated either in voltage or in current control mode, whereas previously published research only considered the rectifier voltage control mode of operation.

The proposed technique provides adequate response to onshore faults, showing recovery times of 200 ms for solid short circuits at the inverter terminals once the fault is cleared. Moreover, the response to 0.8 p.u. voltage sags is similar to that obtained with thyristor-controlled rectifiers. These results represent a substantial improvement over previously published recovery times for HVdc systems with diode rectifiers (larger than 1.5 s) [3]. Moreover, the proposed control system allows for wind farm optimal power tracking and for offshore ac-grid self-start operation.

The proposed control strategy has been validated by considering a wind farm aggregated model, which is generally sufficient to perform stability, fault ride through and voltage and frequency control analysis [13], [14], [16], [17].

On the other hand, the extension of the proposed control strategy to the distributed scenario implies the solution of a number of technical challenges, related to the control of a large number of paralleled inverters, namely voltage and frequency control, active and reactive power sharing, communication of control signals between wind turbines, islanding operation, and stability [29], [30]. However, existing solutions to these problems, such as the use of standard active and reactive power droops [30], [31] or virtual impedances [32], [33], can be readily used to extend the proposed strategy to the control of the individual wind turbines.

Particular attention has been paid to the use of local measurements for the different control algorithms both for normal operation and during transients, to avoid communication related problems and to facilitate the extension of the proposed strategy to the distributed case.

This study has shown that a diode rectifier-based HVdc link represents a technically feasible alternative for the connection of large offshore wind farms with fully rated converters.

APPENDIX

SYSTEM PARAMETERS

A. Wind Turbine

Two-mass model:

Turbine MOI: 10^7 kg·m^2 Frict. coeff: 20 N·m/(rad·s).
Gener. MOI: 10^5 kg·m^2 Frict. coeff: 100 N·m/(rad·s).
Shaft Stiffness $= 160 \times 10^7$ N·m/rad.

PMSG:

Base values: 5000 kVA, 2000 V L-L rms, 20 Hz.
Pole pairs $= 80$; Magnetic strength $= 1.0$ p.u.
$R_s = 0.017$ p.u., $X_l = 0.064$ p.u.
$X_d = 0.8$ p.u., $X_q = 1.0$ p.u.,

DC-link capacitor ($C_{\rm dc}$): 115 kJ, 5.4 kV.

Transformer: (T_W): 1000 MVA/50 Hz , 2/345 (kV L-L rms), $R_W = 0.005$ p.u., $X_W = 0.06$ p.u.

B. Offshore AC Grid

Base values: 193.6 kV L-N rms, 1.745 kA rms, 50 Hz.

C. HVdc Link

Base values: 500 kV , 1000 MW, 50 Hz.

Transformer: (T_R)*:* 603.73 MVA/50 Hz , 345/213 (kV L-L rms), $X_L = 0.18$ p.u.

Filter and reactive compensation bank (C_F, Z_F) (according to the CIGRE benchmark):

$C_F = 2.856$ μF.

Low frequency filter:

$C_{a1} = 5.714$ μF, $C_{a2} = 63.49$ μ F, $R_{a1} = 34.82$ Ω, $R_{a2} = 306.4$ Ω, $L_a = 159.6$mH.

High frequency filter:

$C_b = 5.714$ μF, $R_b = 97.49$ Ω, $L_b = 15.91$ mH.

HVdc-link impedances:

$R_R = R_I = 2.5$ Ω, $L_R = L_I = 0.5968$ H, $C_L = 26$ μF.

D. Controllers

PI current controllers: $K_P = 33.83, K_I = 28.188 \times 10^3$.
PI voltage controller: $K_P = 583.8 \times 10^{-6}, K_I = 0.048$.

REFERENCES

[1] T. Machida, I. Ishikawa, E. Okada, and E. Karasawa, "Control and protection of HVDC systems with diode valve converter," *Electr. Eng. Jpn. (Engl. Transl)*, vol. 98, no. 1, pp. 62–70, 1978.

[2] J. Bowles, "Multiterminal HVDC transmission systems incorporating diode rectifier stations," *IEEE Trans. Power App. Syst.*, vol. PAS-100, no. 4, pp. 1674–1678, Apr. 1981.

[3] S. Hungsasutra and R. Mathur, "Unit connected generator with diode valve rectifier scheme," *IEEE Trans. Power Syst.*, vol. 4, no. 2, pp. 538–543, May 1989.

[4] R. Takagi and T. Nakajima, "A preliminary study on the feasibility of HVDC transmission systems incorporating diode rectifiers and voltage source inverters," in *Proc. IEE Jpn. Annu. Conf. Power Energy Soc.*, 1999, vol. 10, pp. 596–597.

[5] H. Shinohara, T. Shimamura, T. Karube, S. Tanabe, S. I. Tsuruta, K. Takagi, T. Kawachino, I. Kitazaki, and K. Noumi, "A simulation study of a HVDC system for remote island power transmission with a diode rectifier and a self-commutated inverter," in *Proc. IEE Jpn. Papers Tech. Meeting Power Eng.*, 2001, pp. 1–6.

[6] L. Weimers, "HVDC light: A new technology for a better environment," *IEEE Power Eng. Rev.*, vol. 18, no. 8, pp. 19–20, Aug. 1998.

[7] G. Asplund, "Application of HVDC light to power system enhancement," in *Proc. IEEE Power Eng. Soc. Winter Meeting, 2000*, vol. 4, pp. 2498–2503.

[8] P. Bresesti, W. Kling, R. Hendriks, and R. Vailati, "HVDC connection of offshore wind farms to the transmission system," *IEEE Trans. Energy Convers.*, vol. 22, no. 1, pp. 37–43, Mar. 2007.

[9] N. Flourentzou, V. Agelidis, and G. Demetriades, "VSC-based HVDC power transmission systems: An overview," *IEEE Trans. Power Electron.*, vol. 24, no. 3, pp. 592–602, Mar. 2009.
[10] S. Muyeen, R. Takahashi, and J. Tamura, "Operation and control of HVDC-connected offshore wind farm," *IEEE Trans. Sustainable Energy*, vol. 1, no. 1, pp. 30–37, Apr. 2010.
[11] N. Kirby, L. Xu, M. Luckett, and W. Siepmann, "HVDC transmission for large offshore wind farms," *Power Eng. J.*, vol. 16, no. 3, pp. 135–141, 2002 [see also *Power Eng.*].
[12] F. Mura, C. Meyer, and R. D. Doncker, "Stability analysis of High-Power DC grids," *IEEE Trans. Ind. Appl.*, vol. 46, no. 2, pp. 584–592, Mar./Apr. 2010.
[13] R. Li, S. Bozhko, and G. Asher, "Frequency control design for offshore wind farm grid with LCC-HVDC link connection," *IEEE Trans. Power Electron.*, vol. 23, no. 3, pp. 1085–1092, May 2008.
[14] M. Fazeli, S. Bozhko, G. Asher, and L. Yao, "Voltage and frequency control of offshore DFIG-based wind farms with line commutated HVDC connection," in *Proc. 4th IET Conf. Power Electron. Mach. Drives (PEMD)*, 2008, pp. 335–339.
[15] L. Wang, K. Wang, W. Lee, and Z. Chen, "Power-Flow control and stability enhancement of four parallel-operated offshore wind farms using a line-commutated HVDC link," *IEEE Trans. Power Del.*, vol. 25, no. 2, pp. 1190–1202, Apr. 2010.
[16] M. Montilla-DJesus, D. Santos-Martin, S. Arnaltes, and E. Castronuovo, "Optimal operation of offshore wind farms with line-commutated HVDC link connection," *IEEE Trans. Energy Convers.*, vol. 25, no. 2, pp. 504–513, Jun. 2010.
[17] S. Bozhko, G. Asher, R. Li, J. Clare, and L. Yao, "Large offshore DFIG-based wind farm with line-commutated HVDC connection to the main grid: Engineering studies," *IEEE Trans. Energy Convers.*, vol. 23, no. 1, pp. 119–127, Mar. 2008.
[18] M. Fatu, C. Lascu, G. Andreescu, R. Teodorescu, F. Blaabjerg, and I. Boldea, "Voltage sags ride-through of motion sensorless controlled PMSG for wind turbines," in *Conf. Rec. IEEE, 42nd Ind. Appl. Conf. (IAS) Annu. Meeting*, 2007, pp. 171–178.
[19] M. Eichler, P. Maibach, and A. Faulstich, "Full size voltage converters for 5MW offshore wind power generators," in *Proc. Eur. Wind Energy Assoc. (EWEC)*, Brussels, Belgium, 2008, pp. 1–10.
[20] H. Polinder, F. V. D. Pijl, G. D. Vilder, and P. Tavner, "Comparison of direct-drive and geared generator concepts for wind turbines," *IEEE Trans. Energy Convers.*, vol. 21, no. 3, pp. 725–733, Sep. 2006.
[21] F. Blaschke, "The principle of field orientation as applied to the new transvektor closed-loop control system for rotating-field machines," *Siemens Rev.*, vol. 39, no. 5, pp. 217–220, 1972.
[22] A. B. Plunkett, "Field orientation control of a permanent magnet motor," U.S. Classification: 318/254; 318/138 ; International Classification: H02P 600, Mar. 1989.
[23] R. Pena, J. Clare, and G. Asher, "A doubly fed induction generator using back-to-back PWM converters supplying an isolated load from a variable speed wind turbine," *IEE Proc. Electr. Power Appl.*,, vol. 143, no. 5, pp. 380–387, 1996.
[24] R. Cardenas, R. Pena, G. M. Asher, J. Clare, and R. Blasco-Gimenez, "Control strategies for power smoothing using a flywheel driven by a sensorless vector-controlled induction machine operating in a wide speed range," *IEEE Trans. Ind. Electron.*, vol. 51, no. 3, pp. 603–614, Jun. 2004.
[25] R. Blasco-Gimenez, S. Ano-Villalba, J. Rodriguez, V. Aldana, A. Correcher, F. Morant, and E. Quiles, "Variable voltage offshore distribution network for wind farms based on synchronous generators," in *Proc. 20th Int. Conf. Exhib. Electr. Distrib.*, 2009, pp. 1–4.
[26] S. Bozhko, R. Blasco-Gimenez, R. Li, J. Clare, and G. Asher, "Control of offshore DFIG-based wind farm grid with line-commutated HVDC connection," *IEEE Trans. Energy Convers.*, vol. 22, no. 1, pp. 71–78, Mar. 2007.
[27] P. Kundur, *Power System Stability and Control*. New York: McGraw-Hill, Jan. 1994.
[28] M. Szechtman, T. Wess, and C. V. Thio, "First benchmark model for HVDC control studies," *Electra*, vol. 135, no. 4, pp. 54–73, 1991.
[29] M. Chandorkar, D. Divan, and R. Adapa, "Control of parallel connected inverters in standalone AC supply systems," *IEEE Trans. Ind. Appl.*, vol. 29, no. 1, pp. 136–143, Jan./Feb. 1993.
[30] F. Kanellos and N. Hatziargyriou, "Control of variable speed wind turbines in islanded mode of operation," *IEEE Trans. Energy Convers.*, vol. 23, no. 2, pp. 535–543, Jun. 2008.
[31] K. D. Brabandere, B. Bolsens, J. V. den Keybus, A. Woyte, J. Driesen, R. Belmans, and K. Leuven, "A voltage and frequency droop control method for parallel inverters," in *Proc. IEEE 35th Annu. Power Electron. Spec. Conf., (PESC)*,, 2004, vol. 4, pp. 2501–2507.
[32] J. Guerrero, J. Matas, L. de Vicuna, M. Castilla, and J. Miret, "Wireless-Control strategy for parallel operation of distributed-generation inverters," *IEEE Trans. Ind. Electron.*, vol. 53, no. 5, pp. 1461–1470, Oct. 2006.
[33] J. Guerrero, J. Matas, L. G. de Vicuna, M. Castilla, and J. Miret, "Decentralized control for parallel operation of distributed generation inverters using resistive output impedance," *IEEE Trans. Ind. Electron.*, vol. 54, no. 2, pp. 994–1004, Apr. 2007.

Ramon Blasco-Gimenez (S'94–M'96–SM'10) received the B.Eng. degree in electrical engineering from the Universidad Politecnica de Valencia, Valencia, Spain, in 1992, and the Ph.D. degree in electrical and electronic engineering from the University of Nottingham, Nottingham, U.K., in 1996.

From 1992 to 1995, he was a Research Assistant in the Department of Electrical and Electronic Engineering, University of Nottigham. In 1996, he joined the Department of Systems Engineering and Control, Universidad Politecnica de Valencia, where he is currently an Associate Professor. He has been a consultant to Iberdrola Renovables on integration of wind farms in weak grids. His research interests include control of motor drives, wind power generation, and grid integration of renewable energy systems.

Dr. Blasco-Gimenez has been a corecipient of the 2005 IEEE Transactions on Industrial Electronics Best Paper Award. He is a Registered Professional Engineer in Spain, a Chartered Engineer in the U.K., and a member of the Institute of Engineering and Technology.

Salvador Añó-Villalba received the M.Sc. and Ph.D. degrees in electrical engineering from the Universidad Politecnica de Valencia, Valencia, Spain, in 1988 and 1996, respectively.

From 1987 to 1989, he was with the R&D Department of Electronic Traffic S.A. to develop hardware and software for street lighting measuring and automation. In 1988, he joined the Department of Electrical Engineering, Universidad Politecnica de Valencia, where he is currently an Associate Professor. He has been a consultant to Iberdrola S.A. on high-impedance faults, load forecasting, and neutral break detection. His current research interests include wind energy and electrical machines.

Johel Rodríguez-D'Derlée (S'10) received the B.S. degree in electronic engineering from the University of Táchira, Táchira, Venezuela, in 2000 and the M.Sc. degree in math and computer science from the University of Carabobo, Carabobo, Venezuela, in 2004. He is currently working toward the Ph.D. degree at the Institute of Control Systems and Industrial Computing, Universidad Politecnica de Valencia, Valencia, Spain, focusing on advanced control systems for offshore wind farm and HVdc transmission.

His research interests include advanced control techniques for renewable energy.

Soledad Bernal-Perez received the M.Sc. degree in electrical engineering from the Universidad Politecnica de Valencia, Valencia, Spain, in 1999, where she is working toward the Ph.D degree.

Since 2001, she has been a Radio Engineer, carrying out surveys of Global Maritime Distress Safety Systems (GMDSS) radio installations on board of commercial ships for the main Classification Societies. Since 2003, she has also been a Lecturer at the Department of Electrical Engineering, Universitat Politecnica de Valencia. Her research interest include electrical machine drives and grid integration of offshore wind farms using HVdc links.

Francisco Morant received the B.Eng., M.Eng., and Ph.D. degrees in electrical engineering from the Universidad Politècnica de Valencia, Valencia, Spain, in 1976, 1982, and 1985, respectively.

In 1983, he joined the Department of Systems Engineering and Control of the Universidad Politècnica de Valencia, where he is currently a Professor. From 1988 to 1989, he was a Guest Researcher at the Decision and Control Laboratory of Illinois University. He was the Vice President of the Technical University of Valencia (from 1993 to 1995 and 2005 to 2008). His research interests include intelligent control and fault diagnosis.